ENDOR and high-temperature EPR of the N3 centre in natural type Ib diamonds

1992 J. Phys.: Condens. Matter 4 2651

(http://iopscience.iop.org/0953-8984/4/10/027)

J. Phys.: Condens. Matter 4 (1992) 2651–2662. Printed in the UK

ENDOR and high-temperature EPR of the N3 centre in natural type Ib diamonds*

J A van Wyk†, J H N Loubser†, M E Newton‡ and J M Baker‡

† Department of Physics, University of the Witwatersrand, Johannesburg, PO Wits 2050, South Africa

‡ Clarendon Laboratory, Parks Road, Oxford OX1 3PU, UK

Received 16 October 1991

Abstract. The N3 is a single paramagnetic electron centre observed in type Ib diamonds. It has monoclinic symmetry below 200 °C and becomes axially symmetric at higher temperatures. It displays an unusual hyperfine structure which is shown to be from a single ^{14}N nucleus. The spin-Hamiltonian parameters required at higher temperatures have been determined at 550 °C from conventional EPR measurements, whereas the low-symmetry parameters have been determined at room temperature from ENDOR measurements. Some unusual ENDOR and EPR line intensities are explained. The model proposed for the defect involves a substitutional nitrogen as well as a substitutional oxygen.

1. Introduction

The N3 EPR centre was reported for the first time by Shcherbakova *et al* (1972). It frequently occurs along with the P1 (Smith *et al* 1959) and OK1 (Klingsporn *et al* 1970, Newton and Baker 1989) centres in natural type Ib diamond. Its EPR spectra consist of several poorly resolved lines, overlapping the central hyperfine lines of the P1 and OK1 spectra, which complicates the analysis of the spectra.

Shcherbakova *et al* (1972) studied the angular dependence of the lines in the EPR spectrum and interpreted it in terms of a single electron ($S = \frac{1}{2}$) interacting with a nucleus with nuclear spin $I = 1$, presumed to be nitrogen. They tried to represent the EPR spectra of this centre with a spin Hamiltonian of the form

$$\mathcal{H} = \mu_B S \cdot \mathbf{g} \cdot B + S \cdot \mathbf{A} \cdot I. \tag{1}$$

The parameters they determined are given in table 1. The fact that Shcherbakova did not include quadrupole and nuclear Zeeman terms in the Hamiltonian has important implications in interpretation of the EPR spectra and also on the values determined for the spin-Hamiltonian parameters. The magnitudes of these interactions turn out to be comparable to the hyperfine interaction which means that for most directions of the magnetic field B the spectra are more complicated than the simple equally spaced three line spectrum assumed by Shcherbakova. Shcherbakova also remarked

* The N3 centre should not be confused with the optical centre also labelled N3 (Davies 1977) which has been shown to correlate with the P2 EPR centre (Davies *et al* 1977, van Wyk 1982).

0953-8984/92/102651+12$04.50

that the EPR spectrum observed was poorly resolved and that, when the orientation of B changes, the intensity of the lines increases for certain centres with some orientation of principal axes, while for other symmetry-related centres it decreases, these changes not being in accordance with the expected geometrical equiprobable distribution of symmetry-related sites. We show that these changes are due to the striking dependence of the eigenfunctions upon the orientation of B relative to the principal axes of the centres, caused by the relatively large quadrupole and nuclear Zeeman interactions, and that they can be explained once the proper spin Hamiltonian is used and the transitions are correctly identified.

In this paper we report on a new study of the EPR spectra at temperatures between 200 and 600 °C, and on ENDOR studies at room temperature on the N3 centre. These spectra are interpreted in terms of a spin Hamiltonian and a model for the defect is proposed.

2. Experimental details

The measurements were made on a Varian E-line X-band spectrometer using 100 kHz field modulation. A Bruker ER 4114 HT high-temperature cavity was used for the high-temperature EPR measurements, and a Varian large sample access cavity was used for the room temperature ENDOR measurements. The cavity was mounted with its axis horizontal, so that the sample could be rotated through 360° about the horizontal cavity axis, and the magnet through ±20° around a vertical axis. A RF signal from 0.1 to 110 MHz, frequency modulated at about 73 Hz, was passed through a 20 W RF power amplifier and then applied to a parallel-wire single-loop coil inside the cavity. The loop was mounted so that the RF field B_{rf} was perpendicular to both the microwave $B_{\mu\omega}$ and external B fields. The ENDOR information was extracted by applying the unfiltered EPR signal from the 100 kHz phase sensitive detector to a lock-in amplifier tuned to the 73 Hz modulation frequency referred to previously. Owing to the use of two-phase sensitive detectors the second derivative of the absorption signal was recorded.

To observe the ENDOR spectra it was necessary to use microwave powers between 20 and 60 mW, and to adjust the 100 kHz reference voltage 90° from its 'normal' value.

2.1. High-temperature measurements

For several centres in diamond, changes are observed in the EPR spectrum as a function of temperature. For example, at room temperature the P1 centre has axial symmetry around the C–N bond containing the unpaired electron of the defect; whereas at higher temperatures, the paramagnetic electron can tunnel from one C–N bond to the others (Loubser and van Ryneveld 1967, Ammerlaan 1980). A consequence of this is a initial broadening of the EPR lines and a subsequent averaging out of the anisotropic component of the hyperfine interaction to produce an isotropic spectrum consisting of only three hyperfine lines.

The EPR lines of the OK1 centre also begin to broaden at the same temperature as the P1 centre but no averaging of the spectrum is observed. So although the lines are broader at 600 °C the positions of the lines do not change. This shows that even

Table 1. The g-values, hyperfine and quadrupole parameters for the N3 centre, determined by Shcherbacova *et al* (1972), high-temperature EPR and room temperature EPR and ENDOR. For the room temperature data g_z, $A_\parallel$ and $P_\parallel$ lie in the $\{110\}$ plane, and make angle θ with the $\langle 111\rangle$ direction.

Source	g-matrix	A-matrix (MHz)	P-matrix (MHz)	g_N
Shcherbacova *et al* (1972)	$g_z = 2.0024$ $g_x > 2.0024$ $g_y < 2.0025$ $\theta = 35.3°$ $g_x \parallel \langle 1\bar{1}0\rangle$	$A_\parallel = 5.1$ $A_\perp = 1.5$ $\theta = 29.3°$		
EPR at 550 °C	$g_\parallel = 2.00224$ $g_\perp = 2.00236$ (± 0.00005) $g_\parallel \parallel \langle 111\rangle$	$A_\parallel = 4.4$ $A_\perp = 3.8$ (± 0.1) $A_\parallel \parallel \langle 111\rangle$	$P_\parallel = -5.3$ $(\eta = 0)$ (± 0.1) $P_\parallel \parallel \langle 111\rangle$	$g_N = 0.403$
Room temperature ENDOR and EPR	$g_z = 2.0020$ $g_x = 2.0025$ $g_y = 2.0022$ (± 0.0003) $\theta = -32° \pm 5°$ $g_x \parallel \langle 1\bar{1}0\rangle$	$A_\parallel = 4.28$ $A_\perp = 3.12$ (± 0.1) $\theta = 26° \pm 3°$	$P_\parallel = -5.52$ $(\eta = 0)$ (± 0.1) $\theta = 34° \pm 2°$	$g_N = 0.403$

if tunnelling between bonds is taking place, the angles between the bonds and the magnetic field do not change.

The EPR spectrum of the N3 centre at 550 °C, with the magnetic field B applied along a $\langle 111\rangle$ direction is shown in figure 1. The spectrum for the same orientation with the diamond at room temperature is shown in figure 2. Notice that the spectrum simplifies considerably at the higher temperature. This is due to motional averaging which causes the g-matrix, hyperfine and quadrupole interactions to become axially symmetric around the $\langle 111\rangle$ axis. At 550 °C the EPR spectra can be fitted by a spin Hamiltonian ($S = \frac{1}{2}$, $I = 1$)

$$\mathcal{H} = \mu_B g S \cdot B + S \cdot \mathbf{A} \cdot I + P_\parallel [I_z^2 - \tfrac{1}{3} I(I+1)] - \mu_N g_N I \cdot B \qquad (2)$$

with the parameters given in table 1. The spectrum calculated using these parameters is shown in figure 1. Note that the typical three line spectrum for nitrogen is observed only when the magnetic field B is applied along the z-axis of the defect; otherwise strong forbidden transitions are produced by the large quadrupole interaction. It is not obvious from figure 1 that the structure is due to ^{14}N hyperfine interaction; however the subsequent simulation confirms that it is nitrogen.

2.2. *Room temperature ENDOR measurements*

In some natural type Ib diamonds the intensity of the EPR lines of the OK1 and P1 centres at room temperature are reduced after these diamonds have been heated to a temperature above 200 °C, provided that the diamonds are not exposed to light subsequent to the heat treatment. The reduction depends on the anneal temperature and differs from diamond to diamond. The original intensities of the lines can be restored by exposure of the diamond to shorter wavelength visible light. This effect

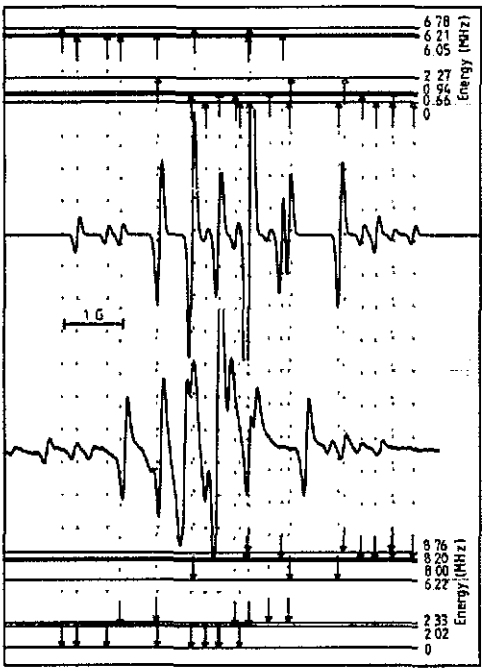

Figure 1. EPR spectra of the N3 centre with the diamond at 550 °C and with the magnetic field applied along a ⟨111⟩ direction. The upper spectrum is calculated using the parameters in table 1, while the lower is the experimental spectrum.

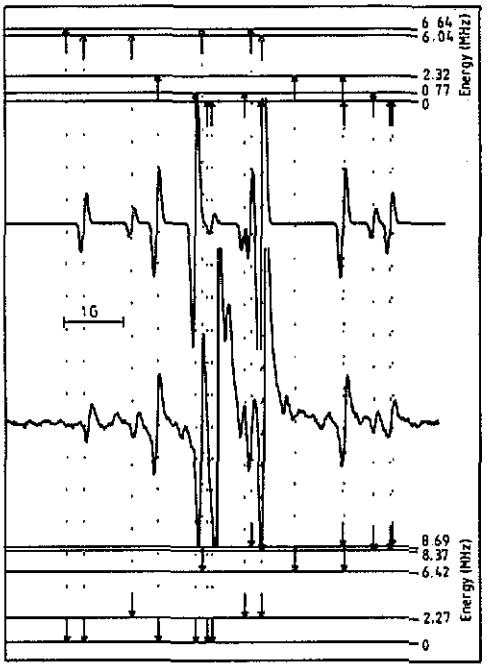

Figure 2. EPR spectra of the N3 centre with the diamond at room temperature and with the magnetic field applied along a ⟨111⟩ direction. The upper spectrum is calculated using the parameters in table 1, while the lower is the experimental spectrum.

can be exploited to reduce confusion caused by overlap of spectra from OK1, P1 and N3.

For measurement of ENDOR of N3, the diamond was first heated to 550 °C to reduce the P1 and OK1 centres as much as possible, and subsequently mounted and transferred to the EPR/ENDOR cavity without exposing it to light.

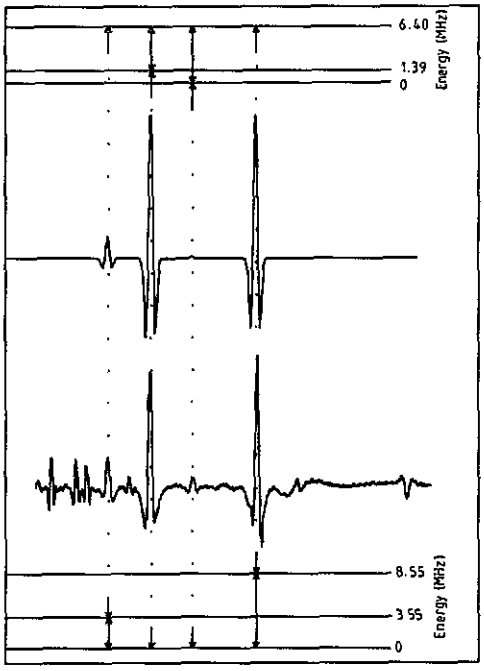

Figure 3. ENDOR spectra of N3 with the magnetic field applied along a ⟨100⟩ direction while saturating the ESR transition $1 \Longleftrightarrow 6$. The upper spectrum is calculated using the approach outlined in section 3, while the lower is the experimental spectrum. Also shown are the hyperfine energy levels for the upper and lower electron spin manifolds (top and bottom respectively).

Typical examples of the ENDOR spectra are shown in figures 3 and 4. Also shown in the figure are the energy levels which are compatible with the observed ENDOR transitions.

The ENDOR spectra exhibited the following somewhat unusual features:

(i) ENDOR transitions could be observed only from the weak EPR transitions (outer lines of the EPR spectrum).

(ii) More ENDOR transitions are observed than are predicted by the usual theory (e.g. Cook 1966). For example, saturating the lowest or highest EPR transitions in figure 2 produces more than the two ENDOR transitions expected for each EPR transition. Two transitions are, however, usually much stronger than the others.

(iii) Also unexpected are the ENDOR transitions with frequencies 11.35 and 13.51 MHz in figure 2. We note that $13.51 \approx 8.53 + 5.0$ and $11.35 \approx 6.41 + 5.0$. In each spectrum the unexpected frequency is equal to the sum of the frequencies of the two more intense ENDOR transitions.

(iv) Other resonances which do not appear to belong to the N3 system are also observed. These are presumably due other defect systems overlapping with the N3 system.

The angular dependence of the ENDOR transitions is shown in figure 5. The EPR and ENDOR measurements were fitted to the spin Hamiltonian ($S = \frac{1}{2}$, $I = 1$)

$$\mathcal{H} = \mu_B S.\mathbf{g} \cdot B + S \cdot \mathbf{A} \cdot I + I \cdot \mathbf{P} \cdot I - \mu_N g_N I \cdot B. \tag{3}$$

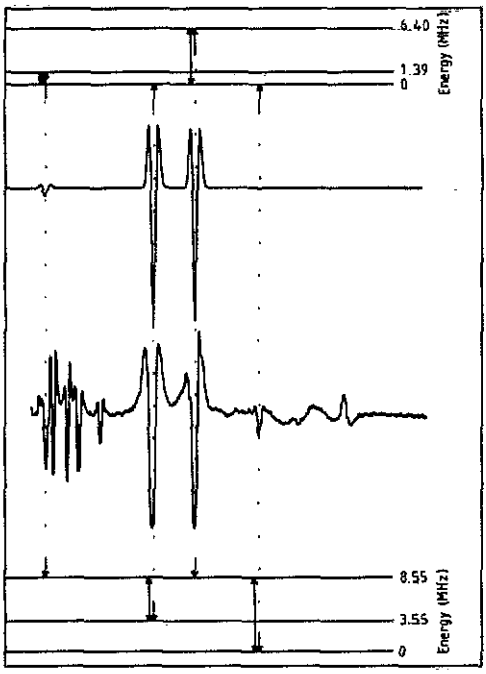

Figure 4. ENDOR spectra of N3 with the magnetic field applied along a ⟨100⟩ direction while saturating the ESR transition 3 ⟺ 4. The upper spectrum is calculated using the approach outlined in section 3, while the lower is the experimental spectrum. Also shown are the hyperfine energy levels for the upper and lower electron spin manifolds (top and bottom respectively).

The complete 6 × 6 secular equation was solved to calculate the ENDOR frequencies. The parameters determined are given in table 1, and the full curves in figure 5 represent the calculated ENDOR frequencies using these parameters. The calculated EPR spectrum with the magnetic field along a ⟨111⟩ axis is shown in figure 2.

3. EPR and ENDOR transition probabilities

When $|g\mu_B B| \gg |A| \gg |P|$, the off-diagonal terms in the energy matrix determined by the spin Hamiltonian (3) are small, M_S and m_I are good quantum numbers, and one observes strong $\Delta M_S = \pm 1$, $\Delta m_I = 0$ allowed transitions and very weak forbidden transitions in EPR. For the N3 centre $|P| \geqslant |A|$ so that the off-diagonal terms in the energy matrix are large, and the forbidden EPR transitions very strong. For the N3 centre the eigenfunctions belonging to each M_S sublevel comprise large admixtures of the $|M_S, +1\rangle$, $|M_S, 0\rangle$, and $|M_S, -1\rangle$ spin states: only along principal directions are the admixtures small. The concept of allowed and forbidden transitions loses all meaning because m_I is no longer a good quantum number. One must use an exact solution of the energy matrix to determine the EPR transition probabilities.

By calculating the matrix elements $\langle \Psi_f | \mathcal{H}' | \Psi_i \rangle$ (Ψ_i, Ψ_f are the eigenfunctions determined by the spin Hamiltonian of the system (equation (3)) and $\mathcal{H}'$ is the Hamiltonian $\mu_B \mathbf{S} \cdot \mathbf{g} \cdot \mathbf{B}_{\mu\omega}$ representing the effect of the perturbing microwave radiation) one can calculate the relative intensities of lines in the EPR spectra, using the spin-Hamiltonian parameters determined from ENDOR. The positions of the EPR transitions are determined from the eigenvalues of the spin Hamiltonian, equation (3). The agreement between the calculated and experimental spectra is good, but there are typically some lines (see figure 3) in the EPR spectra which are not accounted for.

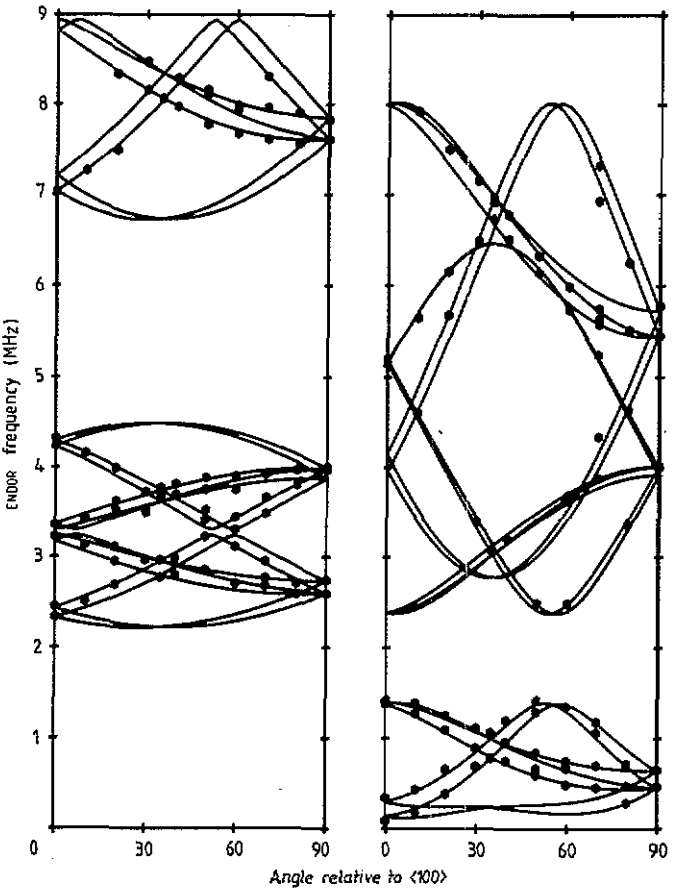

Figure 5. Angular dependence of the ENDOR frequencies in a {110} plane. The ⟨100⟩ axis corresponds to zero angle. The plot on the left represents the angular variations of transitions $1 \Longleftrightarrow 2$, $2 \Longleftrightarrow 3$ and $1 \Longleftrightarrow 3$, while that on the right repesent $4 \Longleftrightarrow 5$, $5 \Longleftrightarrow 6$ and $4 \Longleftrightarrow 6$. The hexagons represent observed frequencies.

These lines are presumed to belong to other centres, and have not been analysed. The EPR transitions intensities are very unusual, because $|P| \geqslant |A|$; and the usual three line nitrogen hyperfine structure is not recognizable from the EPR spectra, as is clearly seen in figures 1 and 2. The transition probabilities of three transitions i.e. $1 \Longleftrightarrow 5$, $2 \Longleftrightarrow 4$ and $3 \Longleftrightarrow 6$ are, however, usually larger than the others.

ENDOR transition intensities are notoriously difficult to calculate. When a RF perturbation $\mathcal{H}'' = \mu_N I \cdot \mathbf{g}_N \cdot \boldsymbol{B}_{rf}$ is applied with $\boldsymbol{B}_{rf}$ in a plane perpendicular to the static magnetic field $\boldsymbol{B}$, transitions can be stimulated between all three hyperfine sub-levels associated with the $M_S = +\frac{1}{2}$, $M_S = -\frac{1}{2}$ levels, because of the strong mixing of the nuclear spin states. Therefore from all the EPR transitions we might be able to see up to six different ENDOR transitions.

In order to see if all six of these transitions are allowed we calculated the matrix elements $\langle \Psi_i | \mathcal{H}'' | \Psi_f \rangle$ produced by $\mathcal{H}''$, when the RF, microwave and static magnetic fields were mutually perpendicular to one another. In general, in agreement with

experiment, we found that all six transitions were permitted, but that the matrix elements varied dramatically with the orientation of the static and RF magnetic fields relative to the principal axes of the defect. The matrix elements alone do not enable us to calculate the ENDOR transition intensities, because the intensities depend on the levels of EPR and RF saturation, and critically on the balance of the various relaxation rates operating in the ENDOR mechanism. However, a matrix element of zero would indicate that the transition is forbidden.

ENDOR mechanisms and relative transition intensities for simple systems are discussed in many texts (for example, Kevan and Kispert 1976). The ENDOR mechanism which we use to explain the N3 ENDOR spectra is often called a ΔT_{1e} mechanism. Using an analogy between relaxation rates, and the resistance of various paths in an electrical circuit, we envisage that the ENDOR response is produced by decreasing the resistance of a path which parallels the spin lattice (T_{1e}) relaxation path; the effective resistance is thus decreased, the level of saturation changed and an ENDOR response is observed.

To facilitate a simple calculation of the approximate relative ENDOR intensities, for comparison with the room temperature data, we made the following assumptions:

(i) Transition probabilities between all nuclear sublevels are such that all the possible transitions are allowed, and they can be saturated with the RF power so equalizing the populations between the connected levels.

(ii) Relaxation rates between different hyperfine levels of the same electron spin state are negligibly slow. This is the situation usually encountered for defects in solids (Abragam and Bleaney 1980).

(iii) Relaxation rates (W_{mn}) between levels Ψ_m and Ψ_n for which $\Delta M_S = \pm 1$ are proportional to the intensity of the EPR transitions between the states, i.e. proportional to the square of the matrix elements produced by the microwave perturbation, ($W_{mn} \propto \langle \Psi_m | \mathcal{H}' | \Psi_n \rangle^2$). This assumption is only valid if direct relaxation processes dominate i.e. when there is a significant phonon density at the energy of the microwave transition. When this is true we can determine the relative importance of the electronic cross-relaxation process because they depend on physically similar processes to the EPR transition probabilities (Abragam and Bleaney 1980). This is a reasonable assumption even at quite high temperatures for defects in diamond.

Now remembering that we are concerned with an $S = \frac{1}{2}$, $I = 1$ system, which has six energy levels, we can express the total effective relaxation rate between any two states, such as Ψ_j and Ψ_k, Ω_{jk} as

$$\Omega_{jk} = W_{jk} + \sum_{\substack{n=1 \\ n \neq j,k}}^{N=6} (W_{jn}^{-1} + W_{nk}^{-1})^{-1} + \text{higher order terms.} \qquad (4)$$

W_{jk} is the direct relaxation path for this transition. Since we have assumed that the relaxation rates between different hyperfine levels of the same electron spin state are effectively zero, it therefore follows for any two states such as Ψ_1 and Ψ_6, $\Omega_{61} \approx W_{61}$. If we saturate the EPR transition between states 1 and 6, the ENDOR signals can be observed when the applied RF field short circuits the relaxation paths $6 \Longleftrightarrow 5$, $6 \Longleftrightarrow 4$, $3 \Longleftrightarrow 1$, $2 \Longleftrightarrow 1$. For example, saturating the $6 \Longleftrightarrow 5$ ENDOR transition increases the effective relaxation rate from $\Omega_{61} \approx W_{61}$ to $\Omega_{61} \approx W_{61} + W_{51}$. This increase in Ω_{61} will produce an enhancement of the EPR signal by a factor of

$(W_{61} + W_{51})/W_{61}$ and hence a maximum ENDOR signal which is W_{51}/W_{61} of the EPR signal. The enhancement can be calculated since we are assuming that the relaxation rates are proportional to the square of the EPR transition matrix elements. Similar calculation may be made for the other transition rates Ω_{jk}.

Determining the transition frequencies from an exact solution of the energy matrix and using the method outlined earlier to determine the relative intensities we simulated ENDOR spectra arising from the $6 \Longleftrightarrow 1$, and $4 \Longleftrightarrow 3$ EPR transitions when the magnetic field $\boldsymbol{B}$ is applied along the $\langle 001 \rangle$ direction, $\boldsymbol{B}_{\mu\omega}$ along the $\langle 110 \rangle$ direction, and $\boldsymbol{B}_{\mathrm{rf}}$ along the $\langle 1\bar{1}0 \rangle$ direction. The experimental and theoretical spectra are compared in figures 3 and 4.

In essence the predictions are correct. For ENDOR from the low-field EPR line ($6 \Longleftrightarrow 1$) theory predicts strong transitions at 5.01 and 8.55 MHz, and weaker ones at 3.55 and 6.41 MHz, in good agreement with the detected transitions. From the high-field line ($4 \Longleftrightarrow 3$) theory predicts strong transitions at 5.00 and 6.41 MHz, and weaker ones at 1.39 and 8.55 MHz, in agreement with experiment. The theory correctly predicts the switch in intensity between the 6.41 and 8.55 MHz ENDOR transitions when observed using the different EPR transitions. The situation is reversed when the transitions $2 \Longleftrightarrow 6$ and $3 \Longleftrightarrow 5$ are saturated. This is empasized in figure 6 in which the ENDOR frequency is kept fixed at 8.55 and 6.41 MHz, while the magnetic field is swept through the EPR spectrum.

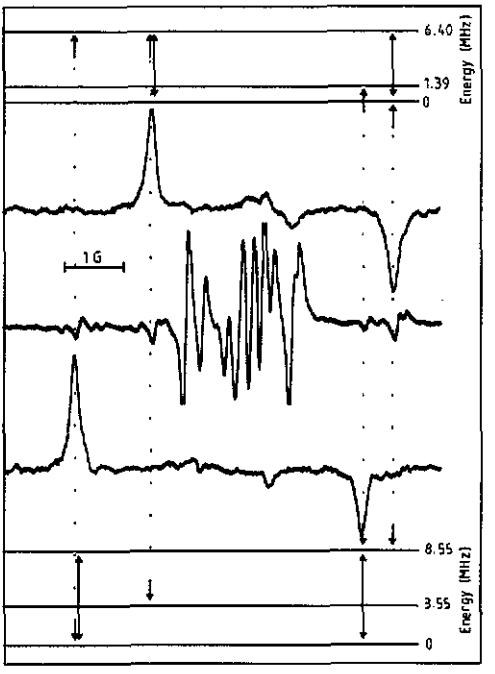

Figure 6. Field swept ENDOR spectra with the magnetic field applied along a $\langle 100 \rangle$ direction. For the upper trace the ENDOR frequency is 6.41 MHz and for the bottom trace it is 8.55 MHz. The EPR spectrum is shown in the middle.

We note in figures 3 and 4 that the computed intensities of the weaker transitions (6.41 MHz resonance line from the low-field EPR line, and the 8.55 MHz line from

the high-field EPR line) are too small. This is because the relaxation rate W_{41} is very slow in comparison with W_{51}, W_{63}, W_{62}, and the approximation that all the relaxation rates between hyperfine levels of the same spin state, are much smaller than W_{41} is not very good. Assuming that these rates may be non-zero, and including the higher order terms in equation (4), will increase the intensities of the small transitions significantly, and decrease the intensities of the large transitions slightly.

ENDOR transitions could not be detected using the strong EPR transitions. With the static magnetic field $\boldsymbol{B}$ along the $\langle 100 \rangle$ direction, $\boldsymbol{B}_{\mu\omega}$ along the $\langle 001 \rangle$ direction and $\boldsymbol{B}_{\mathrm{rf}}$ along $\langle 1\bar{1}0 \rangle$ we calculated the relative intensities of the ENDOR transitions from the strong EPR lines. Calculation showed that the maximum ENDOR signal from the strong EPR lines (i.e. $5 \Longleftrightarrow 1$) was only a few percent of the maximum ENDOR signal from the weak EPR lines (i.e. $6 \Longleftrightarrow 1$), which is consistent with our being unable to detect them.

The good agreement between theoretical and experimental spectra indicates that the assumptions we have made are fairly well justified. It is clear that the N3 ENDOR transitions, although very unusual, can be explained by the strongly mixed states produced by competition between the quadrupole and hyperfine interactions.

In figures 3 and 4 most of the low-frequency lines occur at sub-multiples of the frequency of the strong lines and so may be accounted for as arising from the transitions corresponding to the strong lines stimulated by harmonics of the RF frequency. The lines, of opposite phase, which occur at the sum of the frequencies of the two strong transitions, in figures 3 and 4 have not yet been unambiguously accounted for, though they could correspond to different EPR transitions if the RF were in some way producing a modulation of the microwave frequency.

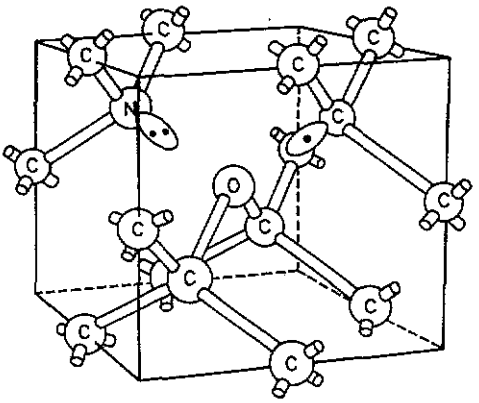

Figure 7. Proposed model for the N3 centre: full electron orbitals on the oxygen are not shown.

4. Discussion and model for the N3 centre

The ENDOR measurements confirm (i) that a $\{110\}$ plane is a principal plane for the defect; and (ii) that the nucleus responsible for the hyperfine structure is nitrogen: this is not immediately obvious from the EPR spectra. The fact that the hyperfine

interaction with the nitrogen nucleus is so small shows that the paramagnetic electron is localized relatively far away from the nitrogen nucleus. Comparison with the hyperfine interaction for unpaired s and p electrons in atomic nitrogen shows that only 1% of the spin density of the unpaired electron is localized on the nitrogen, if only direct hyperfine interaction is considered. The p/s ratio is, however, very similar to that of the P1 centre, demonstrating an equivalence between the orbitals on the N3 and P1 centres. We note, however, that in N3 the symmetry axis of the hyperfine interaction is tilted away from the ⟨111⟩ towards a ⟨110⟩ axis, suggesting some perturbation of the environment of the nitrogen in a {110} plane towards a ⟨110⟩ direction.

In attempting to propose a model for N3, we have a similar situation to that discussed for OK1 by Newton and Baker (1989) in section 4.2: much of that section is relevant to the discussion of N3, so the details will not be repeated here. As for OK1, some perturbation must occur in the {110} plane containing the substitutional nitrogen atom; and as for OK1, it is likely that the perturbation is associated with another substitutional impurity atom in that plane. The lack of resolved hyperfine structure, other than for ^{14}N, indicates that it is an atom with low abundance of isotopes with non-zero nuclear spin. This, together with the fact that Madiba *et al* (1988) have shown that the number of N3 (and OK1) centres is possibly correlated with the oxygen concentration in the sample, implies that the perturbation lowering the symmetry in the N3 defect is probably an oxygen atom.

The properties of N3 and OK1 differ in significant respects: N3 has a larger quadrupole interaction and smaller hyperfine interaction; N3 exhibits motional averaging at high temperatures whereas OK1 does not. All of the arguments about these properties in section 4.2 of Newton and Baker (1989), which led to the rejection of a site nearest to nitrogen for the oxygen atom in OK1, in favour of a second nearest-neighbour site, are reversed for N3. The model shown in figure 7 is consistent with the properties of N3. The nitrogen with five valence electrons is covalently bonded to three carbons with a lone pair in the remaining sp^3 orbital. We propose that the oxygen with six valence electrons forms bonds with two carbons, the remaining four electrons being accommodated in the two remaining p-orbitals. This then leaves an unpaired electron on a carbon atom as shown. This description represents an extreme picture. In practice the unpaired electron will occupy a molecular orbital, with some amplitude on all of the atoms in the region of the defect; but the amplitude on ^{14}N is likely to be small.

The ^{14}N quadrupole interaction of the N3 centre, $P_{\parallel} = -5.52$ MHz at room temperature, is larger than that for any other nitrogen defect in diamond. As the nitrogen is bonded only very weakly to the oxygen in the proposed model, we expect a large axial component in the field gradient giving rise to the large quadrupole interaction.

This model also readily explains the averaging of the spectrum at higher temperature. The oxygen can form bonds with any two of its three nearest-neighbour carbon atoms—the nitrogen being in the fourth nearest-neighbour position. At the higher temperature the bonds can switch from one pair to the other leading to an averaging of the spectrum around the ⟨111⟩ axis containing the nitrogen.

The natural abundance of ^{17}O is too low (0.038%) to permit the confirmation of its presence by observation of oxygen hyperfine structure.

Acknowledgments

The authors would like to thank the management of the Diamond Research Laboratory of the De Beers Industrial Division for providing the diamonds required in this work. We would also like to thank Diamond Research Laboratories and the Condensed Matter Research Unit for their financial support.

References

Abragam A and Bleaney B 1980 *Electron Spin Resonance of Transition Metal Ions* (New York: Dover)
Ammerlaan C A J 1981 *Defects and Radiation Effects in Semiconductors* (Bristol: Institute of Physics) pp 81–94
Cook R J 1966 *J. Sci. Instrum.* **43** 548–53
Davies G 1977 *Chem. Phys. Carbon* **13** 1
Davies G, Welbourn C M and Loubser J H N 1977 *Diamond Research* p 23
Kevan L and Kispert L D 1976 *Electron Spin Double Resonance Spectroscopy* (New York: Wiley)
Klingsporn P E, Bell M D and Leivo W J 1970 *J. Appl. Phys.* **41** 2977–80
Loubser J H N and van Ryneveld W P 1967 *Brit. J. Appl. Phys.* **18** 1029–31
Madiba C P P, Sellschop J P F, van Wyk J A and Annergarn H J 1988 *Diamond Conference (Cambridge)* (De Beers Industrial Diamond Division)
Newton M E and Baker J M 1989 *J. Phys. C: Solid State Phys.* **1** 10549–61
Smith W V, Sorokin P P, Gelles I L and Lasher G J 1959 *Phys. Rev.* **115** 1546–52
Shcherbakova M Ya, Sobolev E V and Nadolinnyi V A 1972 *Sov. Phys.–Dokl.* **17** 513
van Wyk J A 1982 *J. Phys. C: Solid State Phys.* **15** L981–3